International Symposium
On Turbulence and Shear Flow
Phenomena (TSFP-9)
June 30 - July 3, 2015 Melbourne, Australia

MIXING DYNAMICS AND FLUID RESIDENCE TIME IN SPLIT-INJECTION GASEOUS JETS

Dong-hyuk Shin
Faculty of Engineering and the Environment
University of Southampton
Highfield Campus, Southampton, SO17 1BJ, United Kingdom
d.shin@soton.ac.uk

Edward Richardson
Faculty of Engineering and the Environment
University of Southampton
Highfield Campus, Southampton, SO17 1BJ, United Kingdom
e.s.richardson@soton.ac.uk

ABSTRACT

The effects of split-injection on the mixing and the fluid residence time distribution in turbulent gaseous jets are investigated using Direct Numerical Simulation (DNS). The mixing physics identified in this study are important for the understanding of split-injection compression-ignition engine operation, in which mixing rates and fuel residence time control the rate of heat release and pollutant formation. The configuration involves a round turbulent jet issuing from a flat plate, subject to single-pulse, double-pulse, and continuous injection. A novel analysis of fluid residence time is performed by solving a transport equation for the fluid age. A similarity scaling is determined for the residence time in the continuous jet case. It is then shown that the radial gradients of the age of injected fluid are greater in the continuous jet suggesting that, in continuous fuel injection, entrainment of older more-reacted fluid provides a mechanism to promote ignition further upstream compared to pulsed jets. The implications of scalar dissipation and entrainment rate transients for combustion are discussed.

INTRODUCTION

The overall rate of entrainment of ambient fluid into the jet is important in many transient-jet mixing applications. This study is motivated by the application of transient-jets to fuel injection in compression ignition (e.g. Diesel) engines in which scalar dissipation and the fuel residence time are also important factors in the evolution of the combustion process.

Several studies have shown that entrainment is reduced in accelerating jet flow (Kato et al., 1987), and the converse is observed in decelerating jets (Musculus, 2009, and Craske and van Reeuwijk, 2014). These entrainment effects have been attributed to the changing amount of jet fluid and vorticity available to feed the growth of large structures, so that the rate of ambient fluid entrainment adjusts in compensation. Musculus (2009) developed a one dimensional model for the evolution of the cross-stream integrated momentum flux $\dot{M}$ in a decelerating jet. Assuming that the velocity profile in the unsteady-jet remains self-similar and neglecting axial interactions he obtained the following wave equation,

$$\frac{\partial \dot{M}}{\partial t} = -2\alpha \frac{\sqrt{\dot{M}}}{x - x_0} \frac{\partial \dot{M}}{\partial x} \qquad (1)$$

where, x_0 is the origin of the self-similarity and α is $cot(\theta/2)\sqrt{\beta/\rho\pi}$, and θ, β and ρ are the jet spreading angle, the radial velocity shape factor, and the density respectively. Equation 1 predicts that, in the decelerating portion of the jet, the entrainment rate relative to the local concentration of injected fluid is three times greater than in a steady-state turbulent jet. The model is in qualitative agreement with velocity measurements in a gravity-driven water jet (Johari and Paduano, 1997) that imply at least a two-fold increase in the dilution rate in the decelerating region of the jet. The model also explains experimental observations that deceleration waves increase the rate of dilution in Diesel fuel jets (Musculus et al., 2007).

The scalar dissipation rate $\chi_z = 2\mathfrak{D}\nabla Z \cdot \nabla Z$ characterises the local mixing between the jet fluid and the ambient fluid, where Z is the mixture fraction (i.e. a passive scalar with a value of unity in the jet fluid and zero in the ambient fluid) and $\mathfrak{D}$ is the molecular diffusivity of mixture fraction. High values of scalar dissipation rate retard the progress of autoignition (Mastorakos et al., 1997) so that ignition and flame stabilisation usually occur in regions of low scalar dissipation. Recent laboratory measurements illustrate that the scalar dissipation rate is elevated at the leading edge of an impulsively started jet, compared to an equivalent continuous jet (Soulopoulos et al., 2014) but analysis of the scalar dissipation rates during split injection have not been reported based on full-resolution data.

The residence time is important in autoignitive flows since, to leading order, the fluid ignites when the residence time of the most-reactive mixture exceeds the ignition delay time (Mastorakos et al., 1997). Split-injection provides a mechanism through which to modify the

distribution of residence time in an engine and thereby control the location and timing of ignition events during an engine cycle. Split injection presents a challenge for common mixture fraction-based combustion models since mixture fraction does not distinguish between fuel injected at different times. In flamelet modelling, Hasse and Peters (2005) have used two mixture fractions Z_1, Z_2 to indicate fuel from two injections, leading to a two-dimensional flamelet model. We propose an alternative description of residence time using 'age' to indicate when fluid was injected. Age, a, is defined in Enjalbert et al. (2012) by its transport equation:

$$\frac{\partial a}{\partial t} + \vec{u} \cdot \nabla a = \frac{1}{\rho} \nabla \cdot (\rho \mathfrak{D} \nabla a) + 1 \qquad (2)$$

Age is a scalar representing the average residence time of fluid. The fluid's age changes if it mixes with a fluid with a different age according to the molecular mixing term in Eq. 2. Age is a natural reference variable for chemical processes which are kinetically limited, such as autoignition and nitric oxide formation, and it has recently been used as a basis for turbulent combustion modelling (Enjalbert et al, 2012). The jet fluid is assigned zero age as it exits from the injector. Arbitrarily we initialise the age of the ambient fluid equal to zero at time t=0. For purposes of interpretation, the arbitrary contribution of the ambient fluid age can be removed from the transported age to give the average age of the jet fluid, referred to as the *fuel-age*, $a_f = t + (a - t)/Z$. The analysis of fuel age in this study is conditioned on $Z > 0.001$ since the $1/Z$ dependence makes the evaluation of fuel age sensitive to numerical error as Z approaches zero.

SPLIT-INJECTION SIMULATION

The simulation configuration involves a round jet of turbulent fluid issuing from a flat plate into a quiescent atmosphere. The injected fluid is an ideal gas with the same temperature and density as the ambient fluid. The jet Reynolds number is 7,290 and the Mach number is 0.304, based on the volume flow rate. First, a statistically-stationary solution for the near-field of the turbulent jet is obtained by simulating the jet flow for 620 jet times, where the jet time ($\tau = D/U_0$) is defined by the ratio of the jet inlet diameter (D) and the bulk velocity (U_0). The stopping jet simulation is initialized at $t=0$ with the final solution from the statistically-stationary jet simulation and imposing a jet velocity equal to zero. The restarting jet simulation is initialized from the stopping jet solution 20τ after the stopping transient, as illustrated in Fig. 1. Transport equations for two mixture fractions, Z_1, and Z_2 are solved in order to distinguish mass of fluid that is injected before and after the jet is restarted respectively. For comparison with the re-starting jet case, a separate simulation is performed involving an impulsively-started jet issuing into stagnant ambient fluid (not shown in Fig. 1).

The jet inlet mean velocity and mixture fraction have a top-hat profile. The value of the top-hat profile extends until $r = 0.475D$ and smoothly drops to zero following a half cosine function. Away from the jet inlet ($r>0.5D$), a no-slip wall boundary condition is imposed at $x=0$. Pseudo-turbulent velocity fluctuations are superimposed at the inlet using the digital filter method and a low turbulent intensity of 3%. All the other boundaries are non-reflecting outlets (Poinsot and Lele, 1992) with a small buffer region at the downstream outlet boundary. All scalar diffusivities ($\mathfrak{D}$) are assumed equal with unity Lewis number, and the Prandtl number is set equal to 0.72.

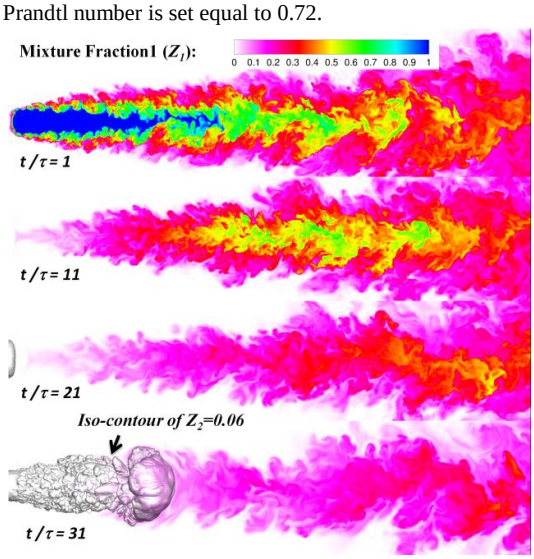

Figure 1. Iso-contour of the second mixture fraction (Z_2=0.06) colored by mixture fraction 1 (Z_1) for the stopping and restarting jet.

The flow is simulated with the compressible DNS code HiPSTAR, developed by the University of Southampton (Sandberg et al. 2014). A fourth-order finite difference scheme (Kennedy et al. 2000) is used in the longitudinal and the radial directions, while the spectral method is used in the circumferential direction. A fourth-order low memory Runge-Kutta scheme (Kennedy et al. 2000) is used for time advancement. In addition, skew-symmetric splitting of the nonlinear terms is used to enhance the stability (Kennedy and Gruber 2008).

For the computational mesh, a stretched grid is used, modified from a previous round jet study (Sandberg et al. 2014). The original grid spacing Δ was refined considering the Reynolds number scaling ($\Delta \sim 1/Re^{3/4}$). In the radial direction, the grid is the most refined near the edge of the jet inlet ($r = D/2$) where the velocity and scalar gradients are the greatest (Sandberg et al. 2014), and 145 points are assigned radially within the jet diameter. In the axial direction, the grid is most refined near the inlet and gradually stretched moving downstream. In the circumferential direction, 64 wave modes are used, corresponding to 130 physical points. The grid consists of $3020 \times 834 \times 130$ structured nodes, spanning axially from $x = 0 - 60D$ and radially from $r = 0 - 30D$.

In order to accelerate the development of the statistically-stationary jet flow field, the flow is simulated for 540τ using a computational mesh with half of the resolution of the final grid. By 540 jet times the first order and the second order statistics in the first 30 diameters of the domain show that the simulation has reached a statistically-stationary state. Then, the half resolved

solution is interpolated onto the final mesh, and the simulation continued over an additional 80τ, confirming that statistical-stationarity is established. The converged turbulent jet simulation also displays self-similarity downstream of ten jet diameters as discussed below.

The simulation results are compared with others reported for the steady state condition. The centreline decay rate constant is 6.7, which is consistent with experimental data (Weisgraber and Liepmann, 1998) concerning a round jet with a top hat velocity profile issuing from a wall. Figure 2 shows the entrainment coefficients defined by Ricou and Spalding (1961). The self-similarity starts to appear from *x>15D*, and the entrainment coefficient matches with the reported data in the self-similar far field of the jet (Ricou and Spalding (1961)).

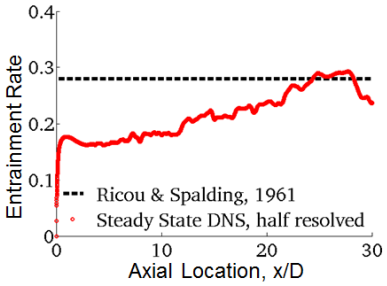

Figure 2. The axial dependence of entrainment coefficient and the far-field value from Ricou and Spalding (1961).

In order to investigate the validity of Musculus's one-dimensional model for entrainment dynamics (Musculus, 2009) Eq. (1) is discretized using a WENO scheme (Jiang and Peng, 2000) and time integrated using a 3rd order Runge-Kutta scheme (Gottlieb and Shu, 1998). Numerical integration of Eq. (1) is necessary for simulation of general injection schemes, whereas the analytical solution presented by Musculus is only applicable when the injection rate decreases linearly.

MASS ENTRAINMENT

The mass flux at a given axial location is evaluated by integrating the axial velocity in the transverse direction out to three half-radii (the half-radius is the radial location where the mean axial velocity falls to half of the centreline mean velocity). Figure 3 shows the axial dependence of the axial mass flux at different times for the new starting jet and the restarting jet. The vortex ring-like flow structure at the head of the jet initially traps a volume of ambient fluid and thereby carries a local maximum of mass flux, however subsequent entrainment is lower than in the steady-state turbulent jet. Figure 3 also illustrates the difference between the new starting jet and the restarting jet. For example, the maximum mass flux at t/τ=25 is 30% greater in the restarted jet compared to the starting jet, and close to the steady-state value. The cause for the difference between the starting and restarting jets can be explained partly by considering Fig. 4.

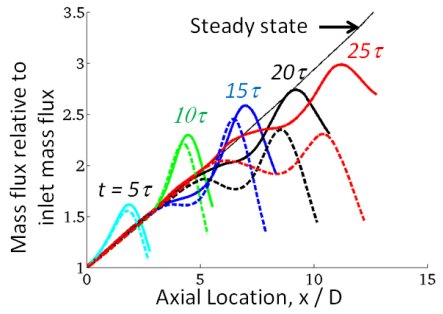

Figure 3. Evolution of the normalized axial mass flux after the (re-)start of injection: dashed lines: new starting jet; solid lines: restarting jet. Injections begin at t=0.

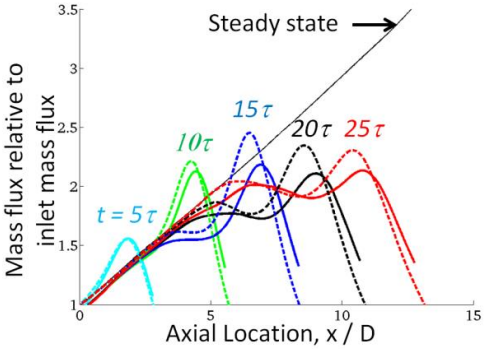

Figure 4. Evolution of the axial mass flux after the (re-)start of injection: dashed lines: new starting jet; solid lines: the mass flux in the stopping jet subtracted from the mass flux in the restarting jet.

Figure 4 shows that subtracting the mass flux in the stopping jet from the mass flux in the restarted jet gives a net mass flux similar to the value in the starting jet. Put another way, the mass flux in the restarting jet is given approximately by summing the mass flux in the wake of the preceding stopping jet and the mass flux obtained from an impulsive jet issuing into a quiescent flow. The remaining differences may be attributed to the residual turbulence and the induced velocity from the preceding injection pulse. Their combined effect is to reduce entrainment into, and to increase the penetration of the restarting jet.

The entrainment rate is given by the axial gradient of the cross-stream integrated mass flux. Figure 5 shows the spatial dependence of the entrainment rate of the stopping jet from the near field of the DNS and from Eq. 1 after adjusting the jet spreading coefficient α to a value that is representative of the jet development in the near field of a steady-jet. Quantitative agreement is not expected because Eq. 1 applies to the self-similar region further downstream in the jet. The simulation of Musculus' model had to start from some distance away from the inlet (x/D=2 in this case) due to 1/x dependency in a model parameter, and an interpolated value from DNS is used for the boundary condition. A qualitative comparison reveals several points. The overall shape of the entrainment rate is similar. In particular, the model predicts the shallow gradient of the entrainment rate in the tail of the deceleration wave. Differences are as follows: The Musculus model shows a sharp peak in entrainment and a sudden drop at the leading

edge of the deceleration wave, while DNS results show a smooth profile with an apparent plateau within the deceleration wave. The Musculus model suggests that the entrainment rate ultimately reaches to 3, while the DNS results indicates that the maximum entrainment rates reaches to 2 at t/tau=7, and starts to decrease subsequently. These differences may be explained in part by the neglect of axial transport in Musculus' model and his assumption that the jet width remains fixed as the entrainment wave passes.

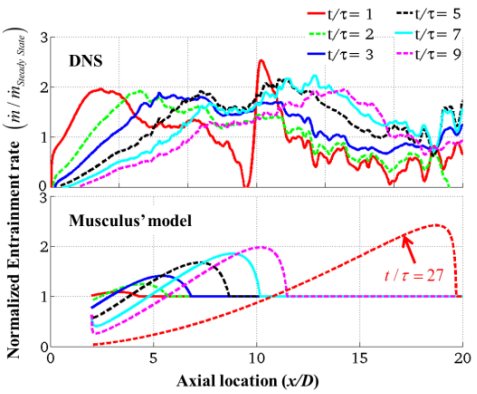

Figure 5. Time evolution of the entrainment rate; (top) DNS results, and (bottom) numerical solution of Musculus's model in Eq. 1 with $\alpha=1$ and $x_{offset}/D=1.2$.

FUEL AGE

Figure 6 shows the radial dependence of the circumferentially-averaged fuel age at multiple downstream locations in the steady-jet. The fuel age increases with axial distance due to the longer convection distance, and with radius, due to the slower convection velocity.

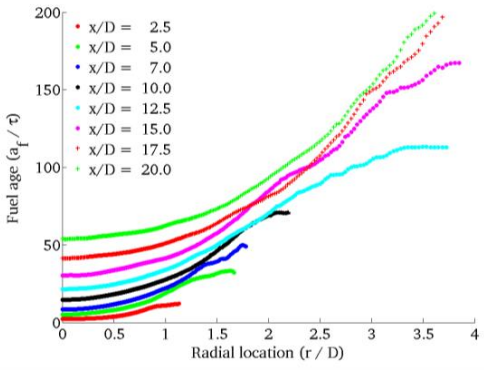

Figure 6. Radial variation of circumferentially-averaged fuel age at different axial locations.

Figure 7 shows the axial dependence of the centreline average axial velocity, mixture fraction, an effective velocity scale based on the average fuel age (x/a_f), and a velocity scale based on the integral of the average centre-line velocity $1/(\int 1/\overline{u_c}dx)$. Downstream of the potential core, the mean centreline axial velocity and mixture fraction display an approximately $1/x$ decay, as expected in a turbulent round jet. The velocity scale based on the integrated centreline velocity provides an estimate for the residence time up to an axial location x that neglects fluid mixing entirely – the result is a substantial overestimate for the effective convection velocity of fuel age. The effective convection velocity of fuel age instead exhibits a $1/x$ decay, and closely follows the profile of the average centreline velocity. The observed $1/x$ decay of the average fuel age at the centreline may be explained by the following three-step argument.

First, a linear model is applied for the conditional velocity $\langle u|\eta\rangle = \langle u|Z=\eta\rangle \sim \eta U_0$ (Klimenko and Bilger, 1999), where $\langle u|\eta\rangle$ represents the conditionally averaged axial velocity at mixture fraction sample-space value η. Second, we make two simplifying assumptions that are justified in the near field of the jet: we neglect mixing of of fuel age in mixture fraction space and neglect axial mixing in the jet. Consequently the conditionally-averaged fuel age is uniform in the cross-stream direction and evolves in the axial direction according to $\langle a_f|\eta;x\rangle \sim \int 1/\langle U|\eta\rangle dx \sim x/(\eta U_0)$. This suggests a $1/\eta$ dependence for the conditionally averaged fuel age, which implies a near-linear variation of fuel age across mixture fraction space for $\eta > 0.4$, so that neglect of mixture fraction-space dissipation is justified at the centreline of the jet in the near field, where the probability $P(Z<0.4)$ is generally small. Furthermore, since the variation of conditionally-averaged fuel age with mixture fraction is near-linear, the unconditional expectation of fuel age can be approximated by $\overline{a_f} \approx \langle a_f|\bar{Z}\rangle$, yielding

$$\overline{a_f} \approx x/(ZU_0). \qquad (3)$$

Axial mixing is known to make a relatively minor contribution to the transport of mixture fraction in turbulent jets, due to the relatively small axial gradient of mixture fraction, however the axial gradient of fuel age is enhanced by source term in Eq. 2. Figure 7 indicates the jet centreline velocity is sufficiently large that mean fuel age varies over a similar axial length scale as the mixture fraction, confirming that it is still reasonable to neglect axial transport effects at the centreline. Third, we note that the mean centreline mixture fraction follows a $1/x$ decay so that $x/(\overline{a_{f,c}}U_0) \approx 1/x$, consistent with Fig. 7.

Equation 3 suggests that the radial dependence of the inverse of fuel age can be related to the radial dependence of the mixture fraction. The radial variation of mean axial velocity and the mean mixture fraction are known to follow self-similar profiles in the fully-developed region of a fully-turbulent jet, and Fig. 8 confirms that this is the case in the present DNS. Figure 8 shows that the radial variation of $\overline{a_{f,c}}/\overline{a_f}$ is self-similar in the region examined and that $\overline{a_{f,c}}/\overline{a_f} \approx \bar{Z}/\overline{Z_{,c}}$ in the region where $r/(x-x_0) < 0.1$, which corresponds approximately to the region in which Eq. 3 is expected to be valid (i.e. $\bar{Z} > 0.3$).

Figure 9 shows the radial profile of fuel age in the continuous injection steady-state, new-starting and restarting injections, at $x/D = 7.5$ and $t/\tau = 15$. In general, the fuel is older at the outside of the jet due to longer residence time in the slower-moving fluid. The centre-line value of fuel-age is similar between cases but,

compared to the single pulse case, the radial gradient of mean fuel age is greater in the continuous jet suggesting that, in Diesel engines, entrainment of older more reacted fluid will promote ignition further upstream in the continuous jet, compared to the pulsed split-injection case.

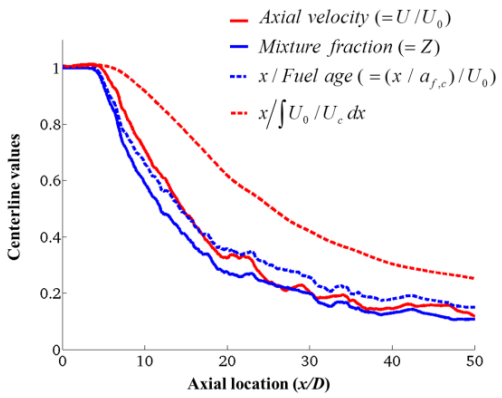

Figure 7. Mean properties in the centre line over axial distance.

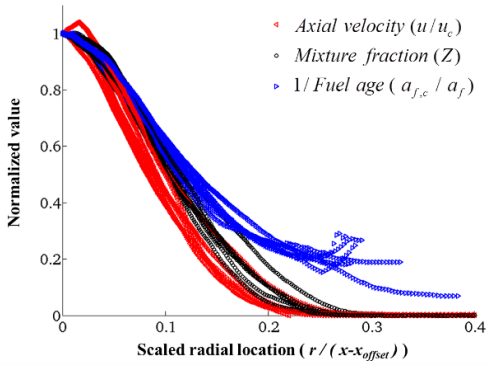

Figure 8. Radial dependence of mean properties in the multiple downstream between x/D = 7.5-20.

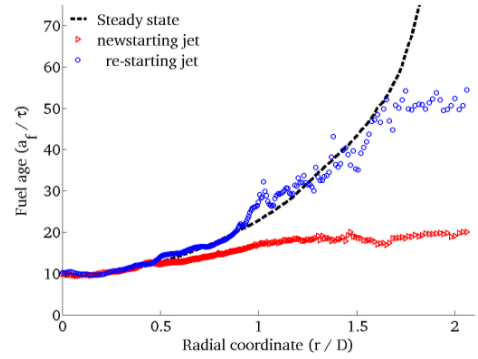

Figure 9. Radial dependence of fuel age for different pulses at $15x/D$.

EVOLUTION OF SCALAR DISSIPATION RATE

Figure 10 shows the scalar dissipation rate on a cross-section through the new starting jet, the restarting jet, and the stopping jet at $t/\tau=15$. A region of low scalar dissipation appears at the core of the starting vortex due to the core of entrained ambient fluid. The structure of the leading vortex is less clear for the restarting jet – possibly because the turbulent flow left in the wake of the stopping jet acts to enhance mixing and to disrupt the propagation of the starting vortex.

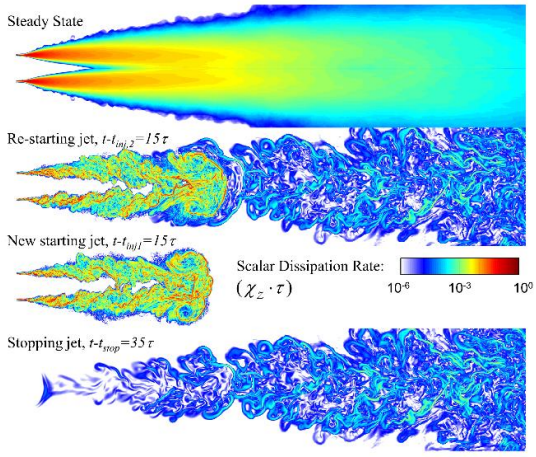

Figure 10. Middle cut of scalar dissipation rate of the steady jet, re-starting jet, new starting jet and the stopping jet.

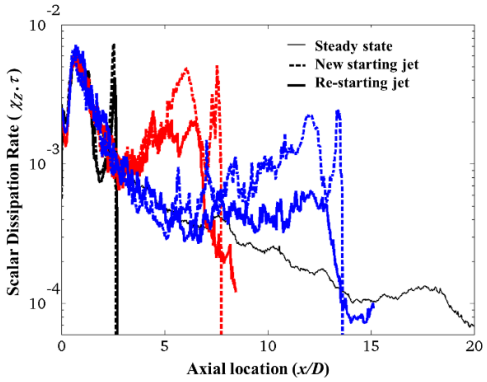

Figure 11. Scalar dissipation rate on the iso-surface of $\bar{Z}$=0.06 in the new starting jet and in the re-starting jet.

Figure 11 shows the evolution of the circumferentially-averaged scalar dissipation rate on the iso-surface where the mean mixture fraction equals 0.06. This mixture fraction iso-surface corresponds to fluid near the exterior of the jet where ignition and flame stabilization tend to occur in Diesel engine fuel jets. Figure 11 also compares the axial variation of the averaged scalar dissipation rate for the continuous jet, the starting jet and the restarting jet. The head of the fuel jet contains higher scalar dissipation rate than steady state condition. However, the scalar dissipation rate evolves towards the steady-state value as the wave of elevated scalar dissipation rate passes.

The scalar dissipation statistics have been computed from one set of flow realizations and they are subject to statistical noise. Noting that Figure 11 is plotted on a logarithmic scale, it is evident however that the scalar dissipation rate at the head of the new starting jet is significantly greater than in the restarting jet, on average. This difference arises because the restarting jet propagates into the wake of the previous stopping jet so that the

restarting jet sees a lower velocity difference compared to the new starting jet, and also because turbulence from the previous stopping jet disrupts structure of the starting vortex and thereby reduces compressive straining of the scalar field. Because the scalar dissipation rate in the restarting jet is less than in the new starting jet, and because the dissipation rate in the wake of the stopping jet is greater than zero, the dissipation rate in the restarting jet cannot be attributed to superposition of the dissipation rates from the stopping jet wake and the new-starting jet. This observation is in contrast to the additive nature of the entrainment dynamics – highlighting the fundamentally different mechanisms that drive the entrainment and scalar dissipation physics.

CONCLUSION

Direct Numerical Simulations comparing different split-injection schedules have been analysed in terms of entrainment effects, the residence time distribution of the jet fluid, and scalar dissipation rates. The analysis shows that entrainment in a starting jet is less than in a steady jet, and that entrainment in a stopping jet is greater than in a steady jet. The findings are in qualitative agreement with a one-dimensional model developed by Musculus (2009), however the profile and magnitude of the entrainment differ from the model predictions. We find that the entrainment in a restarting jet may be estimated by superimposing the entrainment rate in the wake of the previous stopping jet and the entrainment associated with a new-starting jet. The new-starting and re-starting injection transients exhibit scalar dissipation rates one order of magnitude greater than in the continuous injection case. It is observed that the residual turbulence from previous injections affects the coherence of structures in subsequent injection pulses, so that the scalar dissipation rate cannot be estimated from superposition of different injection events, in contrast to entrainment effects.

The residence time distribution for the jet fluid has been analysed by defining a transported scalar quantity called the *fuel age*. A model for the mean distribution of fuel age in a steady-state jet is proposed, explaining the observed $1/x$ axial dependence of centreline fuel age, and self-similarity of the radial fuel age profiles. The fuel age profiles in the new-starting and restarting cases exhibit a flatter radial profile of fuel age. Suggesting that the radial gradient of fuel age during continuous injection may assist ignition and flame stabilisation further upstream in Diesel engine combustion.

ACKNOWLEDGEMENTS

This work has been performed with support from the EPSRC EP/L002698/1, using resources of the UK National High Performance Computing Facility (ARCHER).

REFERENCES

Craske, J., and van Reeuwijk, M., 2015, "Energy dispersion in turbulent jets. Part 1. Direct simulation of steady and unsteady jets", *Journal of Fluid Mechanics*, vol. 763, pp. 500–537.

Enjalbert N., Domingo P. and Vervisch L., 2012, "Mixing time-history effects in Large Eddy Simulation of non-premixed turbulent flames: Flow-Controlled Chemistry Tabulation", *Combustion and Flame*. vol. 159(1), pp. 336 - 352.

Gottlieb, S., and Shu, C.W., 1998, "Total variation diminishing Runge-Kutta schemes", *Mathematics of Computation*, vol. 67, pp. 73–85.

Hasse C. and Peters N., 2005, "A two mixture fraction flamelet model applied to split injections in a DI Diesel engine", *Proc. Combust. Inst.*, Vol. 30(2), pp. 2755-2762.

Jiang, G.S., and Peng, D.P., 2000, "Weighted ENO schemes for Hamilton--Jacobi equations", *Siam Journal on Scientific Computing*, vol. 21(6), pp. 2126–2143.

Johari, H., and Paduano, R., 1997, "Dilution and mixing in an unsteady jet", *Exp. Fluids*, vol. 23, pp. 272–280.

Kato, S.M., Groenewegen, B.C., and Breidenthal, R.E., 1987, "Turbulent mixing in nonsteady jets", *AIAA Journal*, vol. 25, pp. 165–168.

Kennedy, C.A., Carpenter, M.H., Lewis, R.M., 2000, "Low-storage, explicit Runge–Kutta schemes for the compressible Navier–Stokes equations", *Applied Numerical Mathematics*, vol. 35, pp. 177–219.

Kennedy, C.A., Gruber, A., 2008, "Reduced aliasing formulations of the convective terms within the Navier–Stokes equations for a compressible fluid", *Journal of Computational Physics*, vol. 227, pp. 1676–1700.

Klimenko, A.Y., Bilger, R.W., 1999, "Conditional Moment Closure for turbulent combustion" *Prog. Energy Combust. Sci.* 25 595–687.

Lakshminarasimhan, K., Clemens, N. T. and Ezekoye, O. A., 2006, "Characteristics of strongly-forced turbulent jets and non-premixed jet flames", *Exp. Fluids*, vol. 41, pp. 523–542.

Mastorakos, E., Baritaud, T.A., Poinsot, T.J., 1997, "Numerical simulations of autoignition in turbulent mixing flows", *Combustion and Flame*, vol. 109, pp. 198–223.

Musculus, M.P.B., Lachaux, T., Pickett, L.M., and Idicheria, C.A., 2007, "Effects of spray targeting on mixture development and emissions formation in late-injection low-temperature heavy-duty diesel combustion", *SAE Trans.*, vol. 116(3), pp. 515–541.

Musculus M.P.B., 2009, "Entrainment waves in decelerating transient turbulent jets", *Journal of Fluid Mechanics*. vol. 638, pp. 117-140.

Poinsot, T.J., and Lele, S.K., 1992, "Boundary conditions for direct simulations of compressible viscous flows", *Journal of Computational Physics*, vol. 101, pp. 104–129.

Ricou, F.P., and Spalding D.B., 1961, "Measurements of entrainment by axisymmetrical turbulent jets", *Journal of Fluid Mechanics*, vol. 11, pp. 21 – 32.

Sandberg, R., Sandham, and N., Suponitsky, V., 2012, "DNS of compressible pipe flow exiting into a coflow", *International Journal of Heat and Fluid Flow*, vol. 35, pp. 33–44.

Soulopoulos N., Hardalupas Y., and Taylor A., 2014, "Scalar dissipation rate measurements in a starting jet", *Experiments in Fluids*. Vol. 55(3).

Weisgraber, T. H., and Liepmann, D., 1998, "Turbulent structure during transition to self-similarity in a round jet", *Experiments in Fluids*, vol. 24, pp. 210–224.